Journal of Alloys and Compounds 657 (2016) 21–26

Contents lists available at ScienceDirect

Journal of Alloys and Compounds

journal homepage: http://www.elsevier.com/locate/jalcom

# Carrier transport in porous-Si/Ni/c-Si nanostructures

Aleksander K. Fedotov [a], Serghej L. Prischepa [b], Ivan A. Svito [a], Sergey V. Redko [b], Anis Saad [c], Aleksander V. Mazanik [a], Alexei L. Dolgiy [b], Vera V. Fedotova [d], Pawel Zukowski [e], Tomasz N. Koltunowicz [e, *]

[a] Belarusian State University, Minsk, Belarus
[b] Belarusian State University of Informatics and Radioelectronics, Minsk, Belarus
[c] Al-Balqa Applied University, Salt, Jordan
[d] Scientific-Practical Materials Research Center of NAS of Belarus, Minsk, Belarus
[e] Lublin University of Technology, Lublin, Poland

ARTICLE INFO

*Article history:*
Received 16 September 2015
Received in revised form
8 October 2015
Accepted 12 October 2015
Available online xxx

*Keywords:*
Phase transitions in nanocrystalline materials
Electrical properties
Resistance measurement

ABSTRACT

In the present paper we have studied the peculiarities of carrier transport properties of nano-heterostructures containing silicon substrate covered with porous silicon layer, where pores were either filled or non-filled with ferromagnetic Ni clusters. We have carried out DC conductivity experiments as a function of temperature (ranging from 2 to 300 K) and porosity of porous silicon layer (between 30% and 70%). Presence of a surface layer with high resistance on the porous silicon top and its role in nano-heterostructure formation was revealed. It was shown that specific electrochemical kinetics of Ni deposition into porous silicon significantly influences resultant nanostructure resistance and high temperature conductance activation energy.



## 1. Introduction

The study of electrical, magnetic, optoelectronic, thermal and other properties of composite materials, which contain magnetic nanoparticles of the iron group in the insulating or poorly conductive matrix, is of particular interest to modern electronic materials [1,2]. These hybrid materials may serve as the basis for various kinds of sensors [3–5], memory cells [3], optoelectronic devices [6–10], for development of the topological aspects of integrated microcircuits in nanoelectronics [11–13], and some other applications. Porous silicon (PS) with nickel clusters in vertical nanosized pores, which in the case of high density can form nanowires/nanorods, is one of important above mentioned nanocomposite materials. Moreover PS themselves possesses additional unique characteristics because the pores diameters and wall thicknesses can be varied over a wider range than in the case of the porous anodic alumina. In addition, the process of PS manufacturing and its filling with metallic clusters are well compatible with silicon technology in the modern microelectronics.

The electrical properties of PS layers and nanostructures on its base were studied in many papers (see, for example, [14–22]). However the complexity of the atomic structure of PS-based objects did not allow until now to establish an unambiguous correlation between PS porosity, pore sizes, pore wall thicknesses, the type of metal clusters and density of their distribution within the pores, etc. and mechanisms of carrier transport. Fractal models were proposed to describe PS disordered structure in order to explain electrical properties of the PS with different porosity [15–17]. PS was introduced as a material with a band gap gradually decreased with depth in Refs. [18,19]. The structural, luminescent and electrical properties of the PS layers were explained in Refs. [15,19–21] in terms of percolation model [20].

It should also be borne in mind that even the initial PS prepared on single crystalline Si substrate (nanostructure PS/c-Si) structurally should be considered as a multiphase material [22,23] consisting of at least three different phases – c-Si, α-Si:H and $SiO_x$. The deposition of metallic clusters in the pores further complicates the PS layer phase structure, leading to the additional presence of oxides and silicides of the deposited metals in it. An oxide or α-Si:H shells around Si clusters insulate them with each other, and the metallic clusters in the pores can be also surrounded by inclusions

* Corresponding author.
*E-mail address:* t.koltunowicz@pollub.pl (T.N. Koltunowicz).

http://dx.doi.org/10.1016/j.jallcom.2015.10.105
0925-8388/

of their oxides and silicides. As a result, PS carrier transport will be determined by the coexistence of several mechanisms: band mechanism by the silicon substrate on which PS is grown; another one by crystallites of c-Si and silicides inside the PS layer; tunneling of carriers through the barriers at the interfaces, and their hops between semiconducting nanoparticles of the above mentioned c-Si, oxide and silicide precipitates. A special role in the transport of charge carriers may also play a band bending at interfaces resulting in the formation of depleted, enriched or inversion shells around them. It should be noted that the magnetic functionalization of PS due to the presence of Fe-group nanoparticles in nanopores additionally may allow realizing the spin-dependent tunneling of charge carriers in the presence of magnetic field [24].

The aim of this work is to study the mechanisms of charge carrier transport in a wide range of temperatures and porosities in the PS/c-Si and PS/Ni/c-Si nanoheterostructures, where PS layer was formed by means of monocrystalline silicon anodization process and nickel nanoparticles were electrochemically deposited with different densities into vertical nanopores.

## 2. Experimental

We studied electric properties of PS manufactured on pieces of single crystalline silicon wafers doped with Sb (having orientation (100) and room temperature resistivity of 0.01 Ω cm) followed by precipitation of Ni nanoparticles. PS layers were prepared by the anodizing of Si substrate in the dark in solution HF–$H_2O$-Isopropanol (1:3:1 vol.) with anodizing current density $J_{an}$. The used regimes of PS preparation allowed obtaining samples with vary PS porosity and, respectively, with different pore size and wall thickness (see, Table 1). The area of the formed PS/c-Si nanostructures was about 2 $cm^2$. The depth of pores in all series of PS layers was about 10 μm. To obtain nanoheterostructures PS/Ni/c-Si, pores in PS layer were electrochemically filled with clusters of nickel within 5–15 min from the aqueous $NiSO_4$–$NiCl_2$–$H_3BO_3$-saccharin solution with current density $J_{dep} = 3.5$ mA/$cm^2$.

The structure and phase composition of the studied samples were characterized by scanning electron microscopes (SEM) Hitachi S-4800 (Japan) and LEO 1455VP (Germany) supplied with a special X-ray microprobe with energy-dispersive Si:Li detector type of Rontec (MRSA) and also with micro-Raman scattering (RS). MRSA allowed determining the distribution of elements (within ~1%) in the samples. Structure of the studied samples was described in detail earlier in Ref. [25]. μ-RS spectra were recorded on a system with a confocal microscope Nanofinder High-End (Lotis-TII, Belarus–Japan) with a spectral resolution better than 2.5 $cm^{-1}$. RS spectra were excited by a solid-state laser with a wavelength of 532 nm with laser beam power at the sample of about 60 mW. The parameters of sample preparation and their characterization are summarized in Table 1.

Electrical resistance ρ was measured using a 4-probe method in the system with closed-cycle refrigerator (Cryogenics Ltd., England), which allowed to measure ρ($T$) and $I$–$V$ characteristics of nanostructures in the temperature range 2–300 K. Samples for electrical measurements were cut as strips of 2–3 mm width and 7–10 mm in length. On the PS layer surface two current and two potential probes were deposited using ultrasound soldering of In. The indium contacts with the fused copper wires with a diameter of 70–100 μm were used for connecting of working structure to a special contacting platform of measuring probe, which was placed in the cryogenic system. The temperature of the samples was recorded with an accuracy of 0.005 K using a temperature controller 330 Lakeshore. The electrical resistance was measured with an error not exceeding 0.1% using precise Keithley nanovoltmeter with stabilized power supply. Electric measurements were performed using contacts soldered for approximately 1–2 s (type a) and 5–6 s (type b). The samples are denoted as PS-1(a) – PS-15(a) and as PS-1(b) – PS-15(b), accordingly (see Table 1). As shown below, the properties of contacts significantly affected by the duration of the ultrasonic soldering. A total of nine samples of porous silicon were selected for detail $I$–$V$ and $\rho(T)$ measuring. Labels of the samples are given in Table 1.

**Table 1**
Labels of the samples, characteristics of anodizing regimes (current density $J_{an}$ and the anodizing time $t_{an}$) and pore dimension characteristics of PS layers in the initial nanostructures PS/c-Si and after deposition of nickel into the pores PS/Ni/c-Si, during times $t_{dep}$. Activation energy $E_a$ evaluated at $T > 200$ K. Electric contacts were soldered for approximately 1–2 s ($a$) or 5–6 s ($b$).

| PS anodizing regimes and structure | $t_{dep}$, min | Sample label | $E_a$, meV |
|---|---|---|---|
| $J_{an} = 20$ mA/$cm^2$, $t_{an} = 500$ s; | 0 | PS-1(a)/PS-1(b) | 536/- |
| Pore diameter: 20–30 nm | 5 | PS-6(a) | 409 |
| Wall thickness: ~70 nm | 15 | PS-11(a)/PS-11(b) | 26.4/- |
| $J_{an} = 60$ mA/$cm^2$, $t_{an} = 230$ s; | 0 | PS-3(a)/PS-3(b) | 399/349 |
| Pore diameter: 30–40 nm | 5 | PS-8(a) | 284 |
| Wall thickness: ~50 nm | 15 | PS-13(a)/PS-13(b) | 83/- |
| $J_{an} = 100$ mA/$cm^2$, $t_{an} = 180$ s; | 0 | PS-5(a)/PS-5(b) | 227/249 |
| Pore diameter: 70–100 nm | 5 | PS-10(a) | 58.1 |
| Wall thickness: 20–30 nm | 15 | PS-15(a)/PS-15(b) | 386.8/24.1 |

## 3. Results and discussion

### 3.1. PS and PS/Ni layer structure

Examples of cross sections SEM images of PS samples with high porosity at different stages of the pores filling with Ni are shown in Fig. 1. Detailed investigation of the dimensional characteristics of pores and walls and also their distribution by PS layers of different porosity were presented in our previous paper [25]. The example of a RS spectrum for the sample PS-10 with high PS porosity is presented in Fig. 2. Joint analysis of the SEM, MRSA and RS results (together with electric measurements below) allowed to fix the following main features of the initial (PS/c-Si) and filled with Ni (PS/Ni/c-Si) samples. Firstly, we may conclude that the surface of the PS layer is highly amorphized and has charge carriers deficiency on the depths of some hundred nanometers from the surface. We believe that it is due to oxygen excess (see Fig. 2b and c) and strongly disordered structure. In particular, a lighter background near the PS surface at the SEM image in Fig. 1 confirms a poor conductance probably indicating the depletion of space charge region of the PS surface layer. Indirect confirmation of the presence of such highly resistive surface layer on the PS top was also drawn from electric measurements below.

Secondly, as is seen from Figs. 1c and 2c, Ni clusters in the PS pores are located inhomogeneously by pores height. Obviously, the Ni deposition is suppressed on the pore surface, starting only from the depth of 0.5–1 μm, and substantially finishes at the depth of 9.5 μm. Between 1 and 9 μm Ni clusters are incorporated into pores in the form of unconnected droplets and their distribution over the pore depth is more or less uniform. This means that relatively high-resistant regions are present in the PS layer both at the pores top and at their bottom (near the c-Si substrate).

Thirdly, RS measurements in Fig. 2a apparently indicate that before actual deposition of Ni a competitive process occurs resulting in the formation of semiconducting silicide $Ni_2Si$ precipitates.

### 3.2. Electric properties of PS-based nanoheterostructures

This section compares the temperature dependencies of the

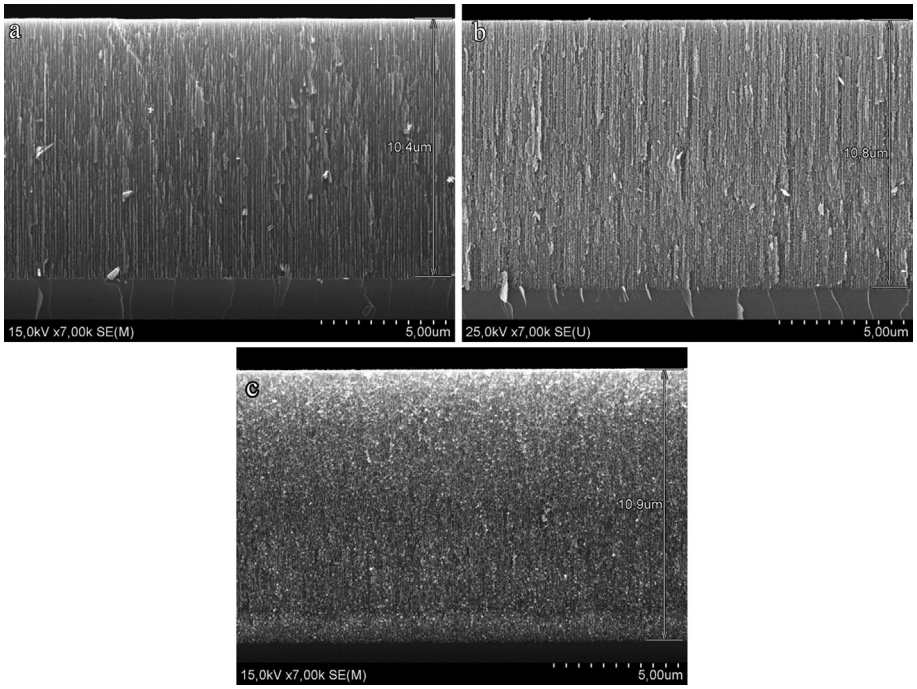


**Fig. 1.** Cross-section SEM images of the PS layers for the PS/c-Si and PS/Ni/c-Si samples from Table 1 with high porosity at different stages of filling of the pores but without soldered In contacts: *a* – PS-5, *b* – PS-10 and *c* – PS-15.

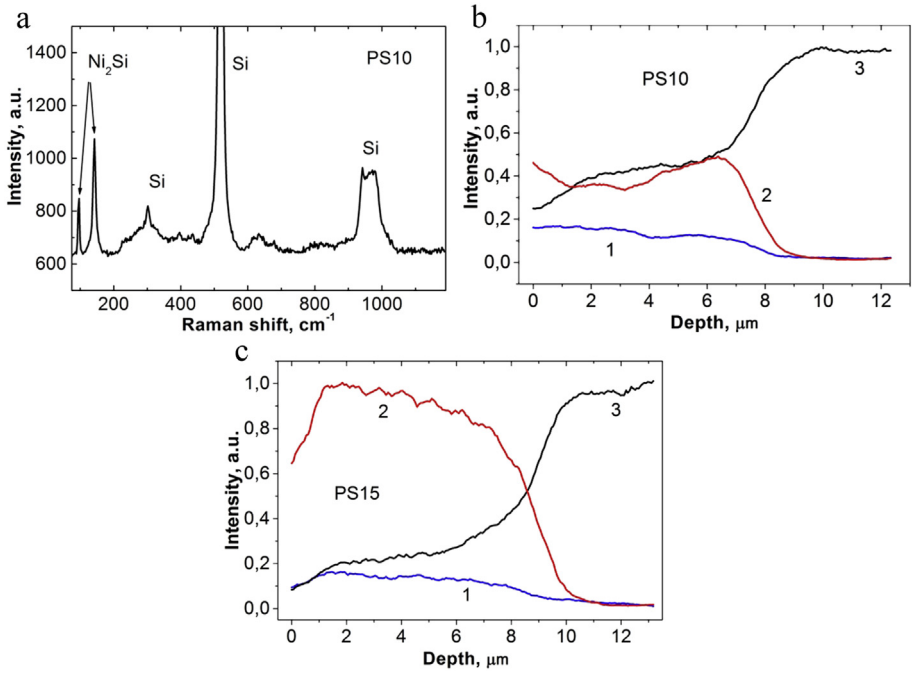


**Fig. 2.** Examples of RS (*a*) and MRSA (*b*, *c*) measurements for the samples PS-10 and PS-15. *1* – oxygen, *2* – nickel, *3* – silicon.

resistivity ρ(*T*) for PS/c-Si and PS/Ni/c-Si samples. Main features of ρ(*T*) curves for the samples with different pore/wall size characteristics, density of nickel clusters in pores (due to different times of deposition $t_{dep}$) and duration $t_{sol}$ of ultrasonic soldering of indium probes to the samples are presented in Fig. 3.

As seen from the comparison of curves with labels (*a*) in Fig. 3a, ρ(*T*) dependencies for non-filled PS/c-Si samples with the shortest times $t_{sol}$ are mostly high-ohmic and have a typical form for the undoped or highly defective (amorphized) semiconductors. These ρ(*T*) dependencies, in particular, show two distinct parts on Arrhenius plots: with a constant activation energy $E_a$ at temperatures higher than 200 K and with a variable $E_a$ at lower temperatures. The $E_a$ values estimated from the slopes of the high-temperature straight-line sections of ρ(*T*) dependencies in coordinates lgρ(*T*)-(1/*T*) are presented in Table 1. As is seen, the largest $E_a$ values are characteristic for the samples with the lowest porosity

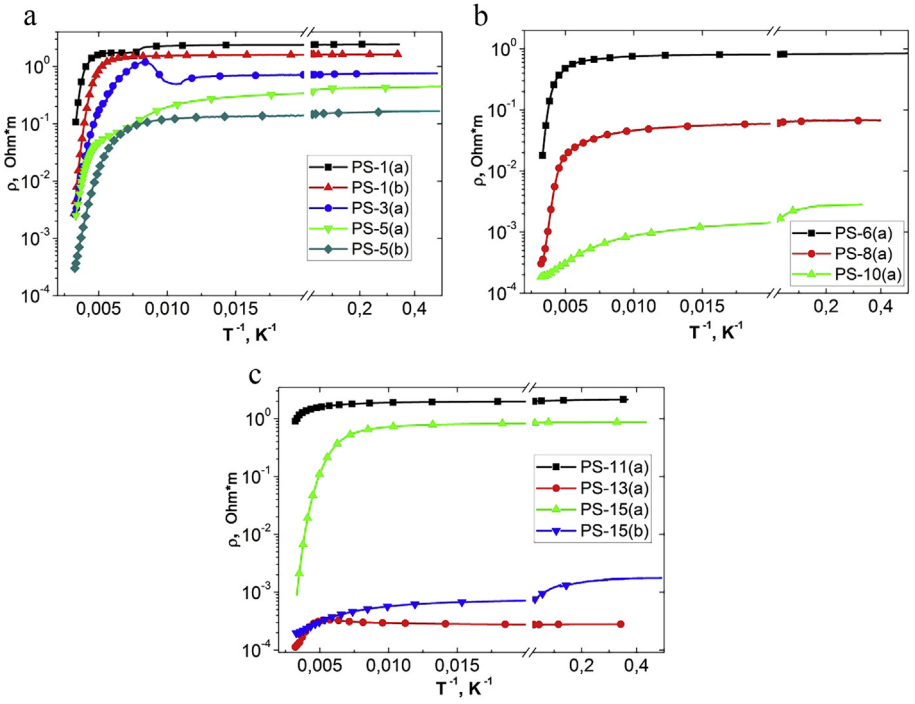


**Fig. 3.** Temperature dependences of resistivity $\rho(T)$ in the Arrhenius scale for the experimental samples with pores non-filled ($a$) and filled ($b$, $c$) with nickel during $t_{dep} = 5$ min ($b$) and $t_{dep} = 15$ min (c) and different durations $t_{sol}$ of ultrasonic soldering of indium contacts. Symbols of samples and labels in curves are denoted in Table 1.

of PS layer, regardless of ultrasonic soldering time $t_{sol}$ of indium contacts. We suggest that $E_a$ values are increased with the thickness of highly resistive PS surface layer. Indeed observation SEM cross-sections of PS has led us to conclusion that the increasing of anodizing current density $J_{an}$ results in thinner PS surface layer with high resistance (see, Fig. 4 below).

It should also be noted that the resistance of the samples PS-1(b) and PS-5(b) with longer $t_{sol}$ times becomes generally lower as compared with similar samples PS-1(a) and PS-5(a) respectively. Taking into account the above-mentioned presence of high-resistive layer at the top (surface) part of PS layer, such behavior can be explained by the following reasons. At longer (more than 2 s) ultrasound exposure of PS surface during the preparation of indium contacts more brittle top surface layer of PS (its thickness was

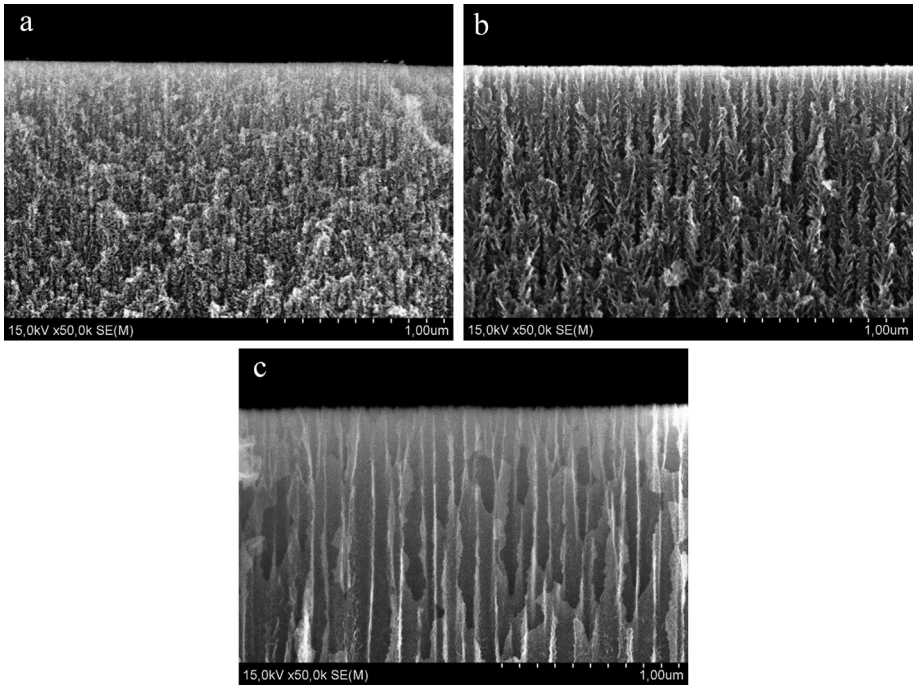


**Fig. 4.** SEM cross-section images of the top region of PS layers for the PS/c-Si samples from Table 1 without soldered In contacts: $a$ – PS-1, $b$ – PS-3 and $c$ – PS-5.

estimated as 20–2000 nm) is likely to completely or partially destroyed by ultrasound subjection. As a result, indium melt is approaching to the more deep and low-ohmic part of PS layer, causing the decrease of measurable PS layer resistance. We also should note that we observed some peculiarities (inflections, steps or maxima) in the behavior of $\rho(T)$ curves in the PS/c-Si samples at approximately 80–150 K when In soldering procedure did not destroy the top high-ohmic layer on PS (compare curves PS-1(a), PS-3(a) and PS-5(a) in Fig. 3a). After a long-time soldering the top layer is destroyed and these anomalies of $\rho(T)$ curves vanished (compare curves PS-1 (b) and PS-5 (b) in Fig. 3a). The high-temperature activation energies of conductance in the samples PS-1(b) and PS-5(b) became lower than in the samples PS-1(a) and PS-5(a), see Table 1. This probably confirms at least double-layer structure of PS layer that was conjectured above when analyzing the PS structure SEM images, MRSA and RS results.

Incorporation of Ni clusters into pores of PS layers generally caused a decrease in the resistance (compare Fig. 3a and b, c) in the whole temperature range as compared with the case of empty pores (Fig. 3b and a). The resistance of the PS/Ni/c-Si samples filled with Ni clusters during 5 min (low density of clusters in pores) is decreased with the increasing pore sizes in the whole temperature range studied, like in the PS/c-Si samples. As follows from Table 1, this is also accompanied by a sharp decrease in the activation energy of the conductance above 200 K. However, the values of the resistance and $E_a$ above 200 K were oppositely increased sharply with the porosity increasing for the PS/Ni/c-Si samples with $t_{dep} = 15$ min and short time of electric probe soldering (compare curves PS-11(a), PS-13(a) and PS-15(a) in Fig. 3c). At the same time, at low temperatures the lowest resistance was observed unexpectedly for the sample PS-13(a) with medium pore diameter, see Fig. 3c. Such effects can be explained in general by specific electrochemical kinetics of Ni deposition into PS mentioned in Ref. [25]. $Ni_2Si$ precedes the Ni deposition and forms a low-resistive ohmic contact to Si. This leaded to lower values of resistance and $E_a$ for a 5 min PS/Ni/c-Si samples as compared with PS/c-Si ones. More long (15 min) filling results in $Ni_2Si$ vanishing and formation of metallic Ni clusters. Nickel itself has a lower resistance than $Ni_2Si$ or Si (sample $\rho$ measured at low temperature decreased) but forms a barrier contact to Si resulting in $E_a$ raising.

Additional experiments are required to identify the exact reasons of different effects of PS layers porosity on $E_a$ and resistance values in the samples with different densities of nickel clusters in the pores. It is a challenging task due to a fundamentally different nature of elements (nickel, silicon, oxygen) and phases (silicon crystallites, α-Si:H, silicides, oxides of Si and Ni, etc.) distribution by the pore depth in the PS samples with different densities of nickel nanoparticles in pores. Furthermore, as follows from the above results of Raman spectroscopy (Fig. 2), one of the reasons for the observed effects may be the formation of nickel silicide precipitates on the walls and at the bottom of pores, because their concentration and distribution by pores depth can significantly affect mechanisms of carrier transport and the total resistance, i.e. $\rho(T)$ and $E_a$.

## 4. Resume

The study of correlation between structure of PS layers (their porosity, density of Ni clusters in pores, pore/wall sizes, etc.) and electrical characteristics of PS/c-Si and PS/Ni/c-Si nanostructures have revealed the following main features:

1. The top of PS layer surface is probably amorphized and/or oxidized resulting in its high resistance which inhibits early plug up of pores by Ni clusters.
2. Peculiar deposition of the nickel, starting from the depth 0.5–1 μm and virtually completed at depth of 9.5 μm, confirms the presence of high-resistive regions both, at the top and at the bottom (near the silicon substrate) of the PS layer.
3. The formation of silicide $Ni_2Si$ precipitates has preceded the deposition of the nickel clusters in the PS.
4. $\rho(T)$ dependencies for PS/c-Si structures have a shape typical for the undoped or highly damaged (amorphized) semiconductors with a constant values of the activation energies at temperatures above 200 K and their variable values at low temperatures.
5. Incorporation of nickel into PS pores generally causes the decrease in the resistance of PS/Ni/c-Si structures with increasing of pore sizes in the entire investigated temperature range and is accompanied by a sharp decrease in the activation energy of conductance above 200 K for the samples filled during 5 min.

## References


[1] S.L. Prischepa, A.L. Dolgiy, H.V. Bandarenka, V.P. Bondarenko, K.I. Yanushkevich, V.G. Bayev, A.A. Maximenko, Yu A. Fedotova, A. Zarzycki, Y. Zabila, Synthesis and properties of Ni nanowires in porous silicon templates, in: L.J. Wilson (Ed.), Nanowires: Synthesis, Electrical Properties and Uses in Biological Systems, Nova Science Publishers, New York, 2014, pp. 89–128.

[2] P. Granitzer, K. Rumpf, Magnetic nanoparticles embedded in a silicon matrix, Materials 4 (5) (2011) 908–928.

[3] J. Verbeeck, O.I. Lebedev, G. Van Tendeloo, L. Cagnon, C. Bougerol, G. Tourillon, Fe and Co nanowires and nanotubes synthesized by template electrodeposition a HRTEM and EELS study, J. Electrochem. Soc. 150 (10) (2003) E468–E471.

[4] K. Liu, K. Nagodawithana, P. Searson, C. Chien, Perpendicular giant magnetoresistance of multilayered Co/Cu nanowires, Phys. Rev. B 51 (11) (1995) 7381.

[5] M. Tsoi, J. Sun, M. Rooks, R. Koch, S. Parkin, Current-driven excitations in magnetic multilayer nanopillars from 4.2 K to 300 K, Phys. Rev. B 69 (10) (2004) 100406.

[6] F. Kozlowski, M. Sauter, P. Steiner, A. Richter, H. Sandmaier, W. Lang, Electroluminescent performance of porous silicon, Thin Solid Films 222 (1) (1992) 196–199.

[7] F. Namavar, H.P. Maruska, N.M. Kalkhoran, Visible electroluminescence from porous silicon np heterojunction diodes, Appl. Phys. Lett. 60 (20) (1992) 2514–2516.

[8] J.P. Zheng, K.L. Jiao, W.P. Shen, W.A. Anderson, H.S. Kwok, Highly sensitive photodetector using porous silicon, Appl. Phys. Lett. 61 (4) (1992) 459–461.

[9] Z. Ye, H. Liu, Z. Luo, H.G. Lee, W. Wu, D.G. Naugle, I. Lyuksyutov, Thickness dependence of the microstructures and magnetic properties of electroplated Co nanowires, Nanotechnology 20 (4) (2009) 045704.

[10] S. Ram, Electrical transport in porous silicon, in: L. Canham (Ed.), Handbook of Porous Silicon, Springer International Publishing, 2014, pp. 263–279.

[11] A.D. Pogrebnyak, V.M. Berestnev, Nanocoatings nanosystems nanotechnologics, Bentham Sci. Publ. (2012) 147.

[12] O.M. Ivasishin, A.D. Pogrebnyak, S.N. Bratushka, Nanostructured Layers and Coating Formed by Ion-plasma Fluxes in Titanium Alloys and Steels, Akademperiodyka, Kiev, 2012, p. 286.

[13] A.D. Pogrebnjak, A.G. Ponomarev, A.P. Shpak, Yu A. Kunitskii, Application of micro-and nanoprobes to the analysis of small-sized 3D materials, nanosystems and nanoobjects, Phys. Uspekhi 55 (3) (2012) 270–300.

[14] V.M. Aroutiounian, M.Z. Ghulinyan, Fractal modeling of porous semiconductors, in: Proc. SPIE 4060, New Trends in Atomic and Molecular Spectroscopy, 1999, pp. 124–135.

[15] V.M. Aroutiounian, M.Z. Ghoolinian, H. Tributsch, Fractal model of a porous semiconductor, Appl. Surf. Sci. 162 (2000) 122–132.

[16] V.M. Aroutiounian, M.Z. Ghulinyan, On the fractal model of the porous layer formation, Mod. Phys. Lett. B 14 (2) (2000) 39–46.

[17] V.M. Aroutiounian, A new model for light emitting structures with a porous material layer, Phys. Status Solidi (a) 165 (1) (1998) 105–109.

[18] M. Ben-Chorin, F. Möller, F. Koch, W. Schirmacher, M. Eberhard, Hopping transport on a fractal: ac conductivity of porous silicon, Phys. Rev. B 51 (4) (1995) 2199.

[19] A.I. Yakimov, N.P. Stepina, A.V. Dvurechenskii, L.A. Shcherbakova, Suppression of the fractal conductivity channel and superlocalization effects in porous a-Si: H, J. Exp. Theor. Phys. 85 (3) (1997) 501–506.

[20] K. Shimakawa, Percolation-controlled electronic properties in microcrystalline silicon: effective medium approach, J. Non Cryst. Solids 266 (2000) 223–226.

[21] V.M. Aroutiounian, M.Z. Ghulinyan, Electrical conductivity mechanisms in porous silicon, Phys. Status Solidi (a) 197 (2) (2003) 462–466.

[22] D. Stauffer, Introduction to Percolation Theory, Taylor & Francis, London, 1985.

[23] E.P. Domashevskaya, V.A. Terekhov, S.Y. Turishchev, D.A. Khoviv, E.V. Parinova, V.A. Skryshevskii, I.V.Garil'chenko, Atomic and electronic structure of the surface of porous silicon layers, Russ. J. Gen. Chem. 80 (6) (2010) 1128–1135.
[24] I. Appelbaum, B. Huang, D.J. Monsma, Electronic measurement and control of spin transport in silicon, Nature 447 (7142) (2007) 295–298.
[25] A. Dolgiy, S.V. Redko, H. Bandarenka, S.L. Prischepa, K. Yanushkevich, P. Nenzi, M. Balucani, V. Bondarenko, Electrochemical deposition and characterization of Ni in mesoporous silicon, J. Electrochem. Soc. 159 (10) (2012) D623–D627.